IEEE Photonics Journal
An IEEE Photonics Society Publication

Tunable Circular Polarization Detection and Full Stokes Measurement Structure

Volume 13, Number 3, June 2021

Bowei Yang
Yuhui Zhang
Mingzhao Ouyang
QiFan Zhu
Yuegang Fu

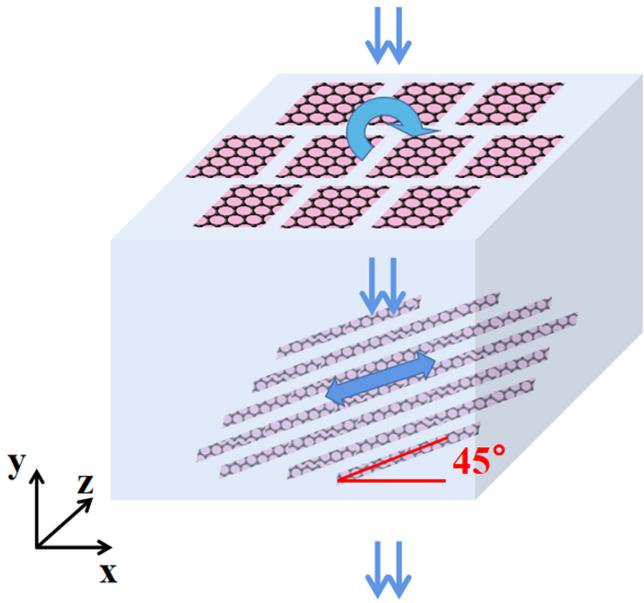

DOI: 10.1109/JPHOT.2021.3075692

Tunable Circular Polarization Detection and Full Stokes Measurement Structure

Bowei Yang,[1] **Yuhui Zhang**,[1] **Mingzhao Ouyang**,[1,2,3] **QiFan Zhu**,[4] **and Yuegang Fu**[1,2,3]

[1]School of Optoelectronic Engineering, Changchun University of Science and Technology, Changchun 130022, China
[2]Key Laboratory of Optoelectronic Measurement and Optical Information Transmission Technology of Ministry of Education, Changchun University of Science and Technology, Changchun 130022, China
[3]Key Laboratory of Advanced Optical System Design and Manufacturing Technology of the Universities of Jilin Province, Changchun 130022, China
[4]College of Physics and Optoelectronic Engineering, Shenzhen University, Shenzhen 518060, China

DOI:10.1109/JPHOT.2021.3075692

Manuscript received March 13, 2021; revised April 17, 2021; accepted April 22, 2021. Date of publication April 27, 2021; date of current version May 31, 2021. This work was supported in part by the National Natural Science Foundation of China (NSFC) (61705018), and in part by foundation for local scientific and technological development guided by the central government of China (202002037jc) and 111 Project of China (D21009, D17017). Corresponding author: Yuegang Fu (e-mail: fuyg@cust.edu.cn).
This article has supplementary downloadable material available at https://doi.org/10.1109/JPHOT.2021.3075692 provided by the authors.

Abstract: Measuring the polarization state of light is an inherent problem, especially for the detection of circularly polarized light. We propose a metasurface structure based on graphene to investigate the circular polarization detection function in the THz regime by using the finite difference time domain (FDTD) method. The proposed graphene metasurface consists of a layer of graphene arrays, a polymer dielectric spacer, and a layer of graphene bands. By adjusting the Fermi energy, the structure can realize tunable polarization detection functions. On this basis, we combine tunable filters with different angles into the structure to achieve full Stokes parameter measurement. The simulation results show that the structure's working band can be tuned in the range of 25.88 μm-28.68 μm. The structure we designed helps to develop a tunable and integrated polarization detection method.

Index Terms: Graphene metasurface, tunable polarization detection, full Stokes measurement.

1. Introduction

The polarization of light is one of its basic attributes [1]. Polarization detection technology can realize cancer detection [2], [3], aerosol characterization [4], [5], and image enhancement [6], [7] and is widely used in various fields. Therefore, the research of polarization detection devices is significant.

Arranged polarizers consecutively placed in front of the detector properly can obtain the Stokes parameters [8], [9]. This method is complicated, and the optical system is huge, especially the detection method of circularly polarized light is more complicated [10]. In recent years, metasurfaces for polarization detection have been proposed. The team of M. Khorasaninejad reported on

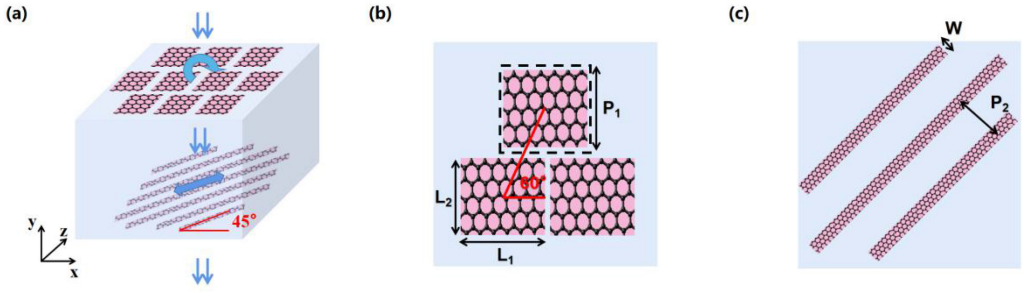

Fig. 1. (a) Schematic diagram of the circularly polarized detection structure consisting of a rectangular graphene array and a graphene energy band group layer. (b) The top view of the top layer of graphene arrays. $P_1 = 800$ nm, $L_1 = 760$ nm, $L_2 = 720$ nm, (c) The top view of the bottom layer of graphene bands. $P_2 = 565$ nm, $W = 330$ nm.

multispectral chiral imaging with a metalens, which achieved separate focusing of left and right polarized light at a wavelength of 532nm [11]. The Pin Chieh Wu team reported visible metasurfaces for on-chip polarimetry, which achieved complete Stokes parameter detection in the visible light band [12]. The Ali Basiri team reported a polarization detection structure based on the principle of shrimp eyes, which achieved a transmission efficiency of more than 80% at the wavelength of 1.47um, and they also proposed a full Stokes detection structure [13]. These studies greatly promoted the miniaturization of polarization detection devices. However, the center wavelength of these structures is fixed. When the actual wavelength is far from the center wavelength, the efficiency of the structure will decrease, and the error will become larger. This greatly limits the practical application of polarization detection metasurfaces.

To solve the above problems, we propose a tunable spectral polarization detection structure. By adjusting the Fermi energy of graphene, the working wavelength of the structure can be adjusted [14], [15]. Therefore, more polarization information in the spectral dimensions can be obtained. The transmittance difference in the working spectal is very small. We have also proposed a full Stokes detection structure, which is also tunable, and each layer can work independently. We integrate six detection elements into two structures, which can be used to develop high-resolution polarization detection devices. We proposed structure can provide an improved method of Tunable polarization detection.

2. Structure Design and Theoretical Analysis

2.1 Principle of Circular Polarization Detection Structure

Fig. 1(a) shows the schematic diagram of the proposed tunable circular polarization detection structure, which is designed to distinguish the direction of rotation of circularly polarized light. The graphene layer on the bottom of the structure acts as a polarization filter. The graphene layer on the top of the structure acts as a quarter-wave plate. The graphene materials used are all monolayer graphene. A dielectric substrate layer separates the two graphene layers, the permittivity of the dielectric substrate is assumed to 2.25. In the simulation, the thickness of the proposed structure is set to 3 μm, which can be adjusted according to actual needs. When the incidence is right circularly polarized light(RCPL), the incidence can be modulated into linearly polarized light after passing through the quarter-wave plate, and the polarization angle with the x-axis is 45°, then the light can pass through the bottom graphene layer. If the incidence is left circularly polarized light (LCPL), the polarization angle of the outgoing is 135° and the light cannot pass through the bottom graphene layer.

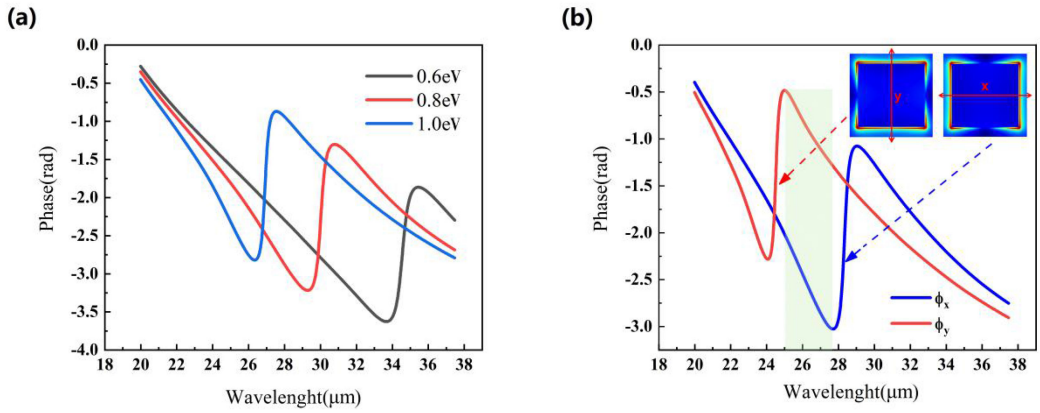

Fig. 2. (a)Phase of x-polarized light at different Fermi energies (b)The electric field and phase of x and y polarized light.

2.2 Principle of Tunable Graphene Quarter-Wave Plate

Fig. 1(b) shows the top view of the proposed structure, where P1 represents the length of one unit cell, L1and L2 represents the length and width of the graphene patch. In the y-direction, two adjacent cells are arranged at 60°. The monolayer graphene is characterized by surface conductivity, which can be simplified in THz frequency to a Drude-like expression:

$$\sigma_g = e^2 E_F i/\pi\hbar^2(\omega + i\tau^{-1})$$

where ω is the working radian frequency, e is electron charge, $\hbar$ is reduced Planck's constant, E_F is the Fermi energy, and τ is the electron-photon relaxation time. In our study, τ is assumed to be 10^{12}s [16]. The resonant frequency of the periodic rectangular graphene patch is affected by its length L and Fermi energy EF, which follow the expression [17]:

$$f \propto \sqrt{E_F/L}$$

The working wavelength of the structure can vary with Fermi energy. The different Fermi energies of graphene ribbons between 0 and 1eV can be achieved by tuning the gate voltages.

We simulate the phase delay of x-polarized light, Fig. 2(a) shows the phase delay with different Fermi energies, the increase of Fermi energy will shift the working wavelength. Circularly polarized light is considered to be composed of x and y polarized light; the x and y polarized light are equal in intensity and have a phase difference of $\pi/2$. When the phase difference is modulated to 0 or π(phase difference increases or decreases by $\pi/2$), circularly polarized light is modulated to linearly polarized light.

We design graphene cells of the top layer with different length and width so that the response wavelengths of polarized light in x and y directions are different. Fig. 2(b) shows the phase delay with the incidence of x-and y-polarized and the insets are the electric field distributions. The electric field diagram shows that X and Y polarized light excites surface excitons at the edges of graphene, resulting in phase delay. In the marked region, the two lines of polarized light produce a phase difference of $\pi/2$, which conforms to the working principle of quarter-wave plate.

2.3 Principle of Tunable Graphene Polarization Filter

We design the bottom graphene gratings to be polarization filters. Fig. 1(c) shows the top view of the bottom layer of graphene bands, where W represents the width of the graphene band. Graphene bands are set 45° along x-direction. In the simulation, we assume that the graphene strip is parallel to the x-axis and simulates the case of x-and y-polarized light incidence. Fig. 3(a) shows the electric field in the graphene band, we can see that y-polarized light excites strong surface excitations, while

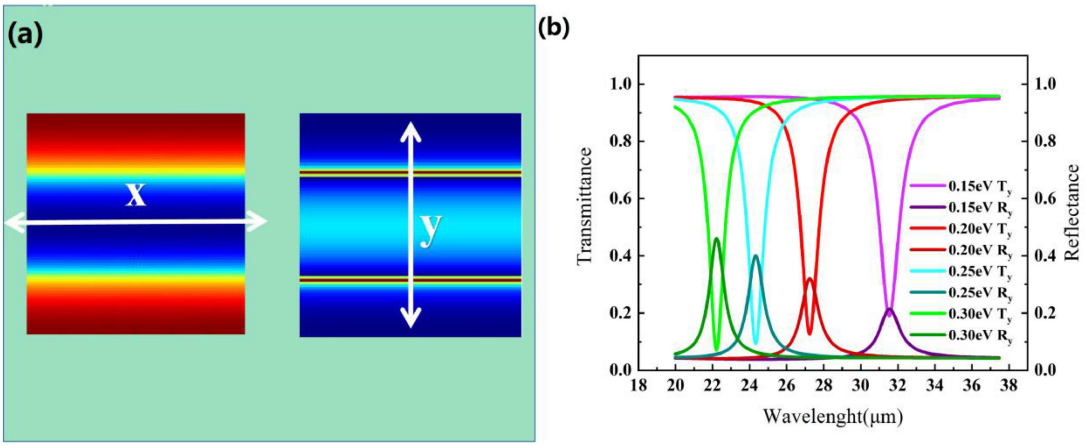

Fig. 3. (a)The electric field of the graphene band. (b)Transmittance and reflectance at different Fermi energies.

x-polarized light does not. Therefore, the light perpendicular to the direction of the graphene band will be filtered. Fig. 3(b) shows the transmittance and reflectance of y-polarized incidence when the Fermi energy of the graphene band is adjusted. As the Fermi energy is increased, the operating wavelength is shifted, the filtering effect is enhanced, and the reflectivity is increased.

3. Results and Discussion

3.1 Circular Polarization Detection Structure Simulation

We first design the structure as a quarter-wave plate by using FDTD solution. We choose to set the Fermi energy to 0.9eV in order to produce enough phase delay. In the simulation, the source is set to x-and y-polarized light with a phase difference of $\pi/2$ (Simulate LCPL and RCPL, respectively.). In Fig. 4, T_x and T_y represent the transmission with different wavelengths, $\Delta\phi$ is the phase difference between x-and y-polarized incidence. As we can see, the transmission of two orthogonal linear polarized incident waves are the same, the phase difference of RCPL is close to zero and the phase difference of LCPL is close to $\pi/2$ at 27.23 μm wavelength. It shows that the graphene array functions as a quarter-wave plate and circularly polarized light is converted into linearly polarized light.

Fig. 4(d) shows the transmission efficiency of the quarter-wave plate. The transmittance of the structure can reach 50.57%. At the same time, the reflectivity is 43.76%. In order to reduce the error caused by mutual reflection between the two-layer of graphene, it is necessary to reduce the reflectivity of the lower layer filter.

We simulate the effects of the period and alignment Angles of graphene patches on phase delay and transmittance. To investigate the effect of alignment Angles, we defined the difference between the centers of the upper and lower graphene patches in the x-direction as Δx. Fig. 5 shows the simulation results. When the period increases, the resonance position has a blue shift, transmissibility decreases. In Fig. 5(c), the phase curves of Y-polarized light coincide. The cross arrangement of graphene patches in the X direction slightly affects the resonant wavelength of X-polarized light. The transmissivity of cross-arranged structures is higher.

We can get less reflect light by choosing a low Fermi energy for the graphene ribbon. In the simulation, we find that when the Fermi energy is 0.2eV, the center wavelength is 27.23 μm. Fig. 6(a) shows the transmission efficiency of the filter. T_x and R_x represent the transmittance and reflectance of X-polarized light. T_y and R_y represent the transmittance and reflectance of Y-polarized light. The transmittance of incident light parallel to the graphene ribbon exceeds 96% and the transmittance of light perpendicular to the graphene ribbon is only 12%. The reflectivity

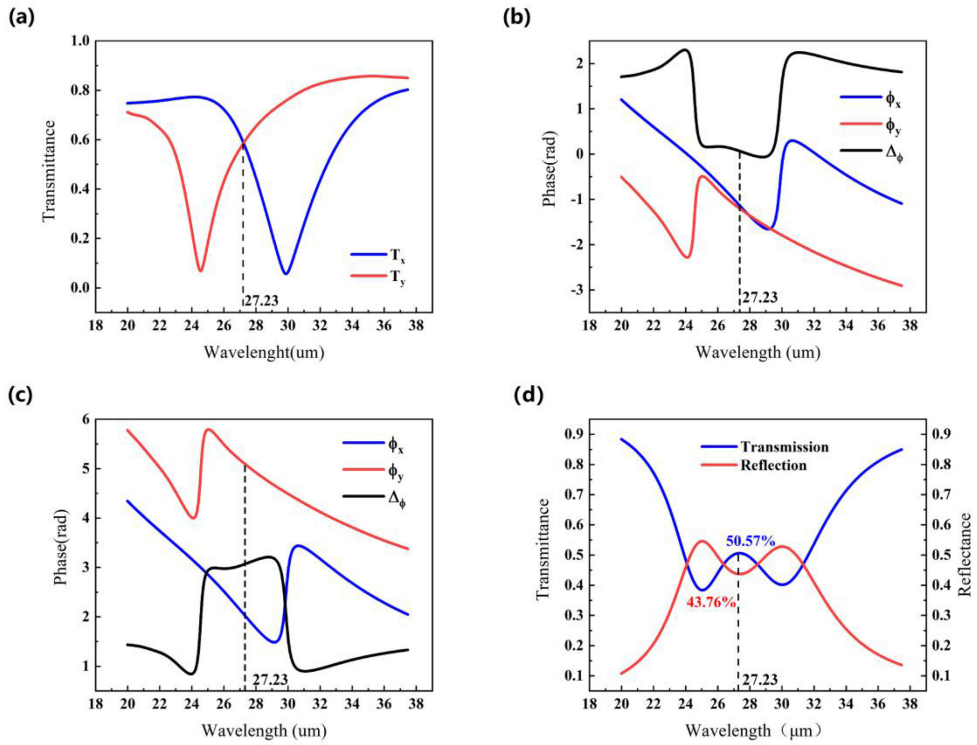

Fig. 4. (a)Transmission coefficient when Fermi energy is 0.9eV. (b) Phase information of RCPL incident. (c) Phase information of LCPL incident. (d) Efficiency of the quarter-wave slice.

of the filter is suppressed 30%. The error caused by reflection does not affect the function of the structure. Finally, we perform the overall efficiency simulation. Fig. 6(b) shows the transmission efficiency of RCPL and LCPL at the wavelength of 27.23 μm, which the transmission rate of RCPL is 50.94%. The transmission rate of LCPL is 7.85%. It shows that the structure we designed can discriminate CPL well.

3.2 Structural Tunability Simulation

Next we verify the tunability of the structure. The operating wavelength of the structure can be changed by changing the Fermi energy of graphene. The transmission efficiency of the structure will also be slightly affected, but it does not affect the function of the structure. We set the Fermi energy of the graphene array to 0.8eV and 1.0eV. Fig. 7 shows the simulation results with the incidence of RCPL.

When the Fermi energy is 0.8eV, the resonance position has a red shift. The transmission coefficients of both orthogonal linear polarized incident waves are the same at 28.68 μm wavelength.Fig. 7(b) shows the phase information. After changing the Fermi energy, the phase curves of X and Y polarized light can still intersect. We label the positions where the phase difference is close to 0. The phase difference still can be modulated to 0. So the quarter-wave plate is still effective. When the Fermi energy is 1.0eV, the resonance position has a blue shift. The transmission coefficients of both orthogonal linear polarized incident waves are the same at 25.88 μm wavelength. The phase difference still can be modulated to 0. So the quarter-wave plate is still effective. In a word, the quarter-wave plate we designed is still effective after changing the Fermi energy. Next, we are going to find the corresponding Fermi energy of the filter. Fig. 8 shows the efficiency of the filter. When the Fermi energy is adjusted to 0.181eV, the center wavelength is

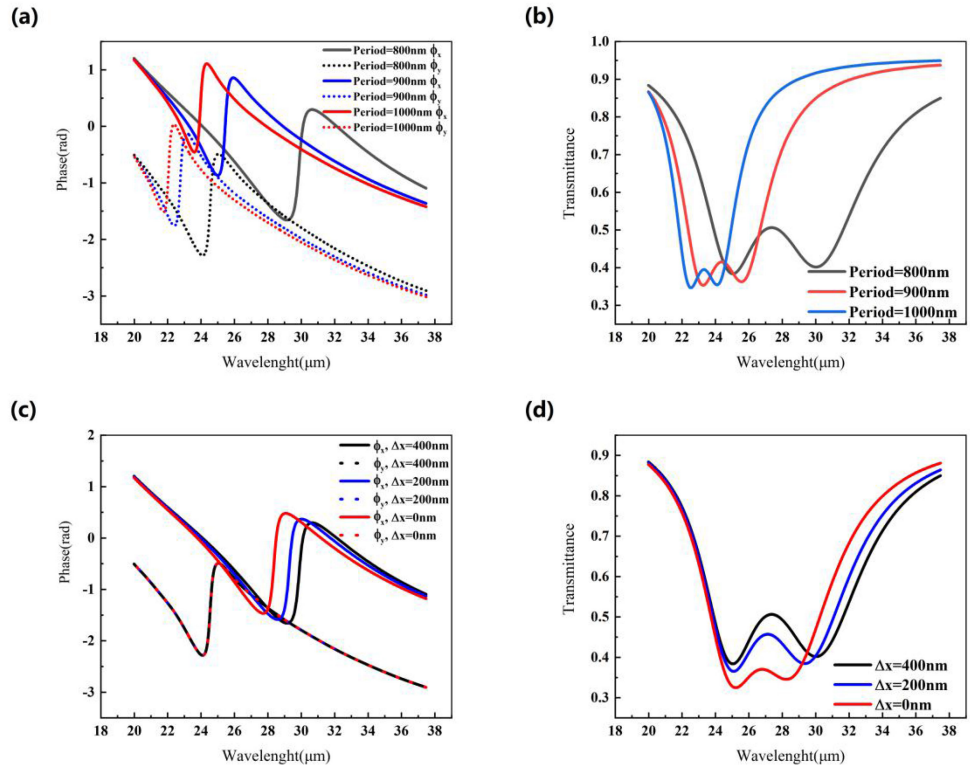

Fig. 5. (a) The effect of period on phase. (b) The effect of period on transmittance. (c) The effect of alignment Angle on phase. (d) The effect of alignment Angle on transmittance.

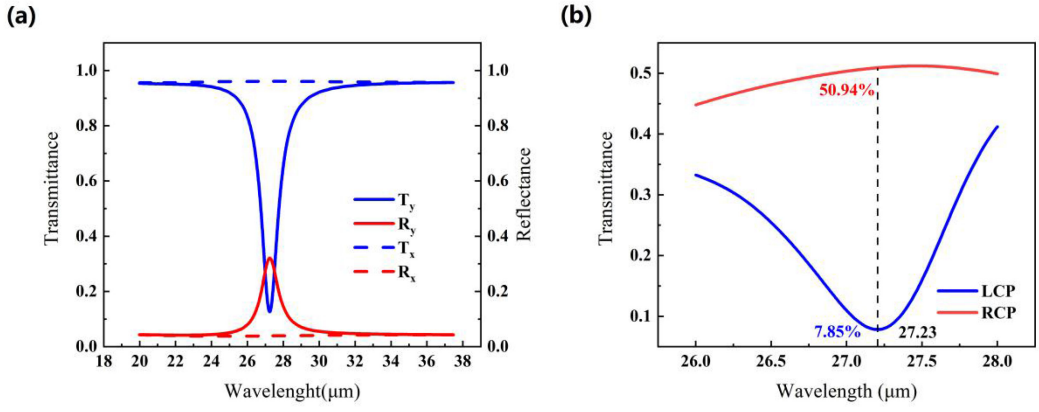

Fig. 6. (a) Efficiency of the filter at 0.2 Fermi energy. (b) Transmission efficiency of circular polarization detection structure.

close to 28.68 μm. When the Fermi energy is adjusted to 0.221eV, the center wavelength is close to 25.88 μm. We keep the top and bottom layers working at the same wavelength.

We try to spread the working wavelength wider. We set the Fermi energy to 0.7eV. Fig. 9 shows the phase information. At this case, the phase delay is not sufficient to modulate the difference to 0. The Fermi energy of the upper graphene can be adjusted between 0.8eV and 1.0eV. The Fermi energy of the lower graphene can be adjusted between 0.181eV and 0.221eV. The center wavelength of the two-layer structure are the same, and the efficiency will not decrease.

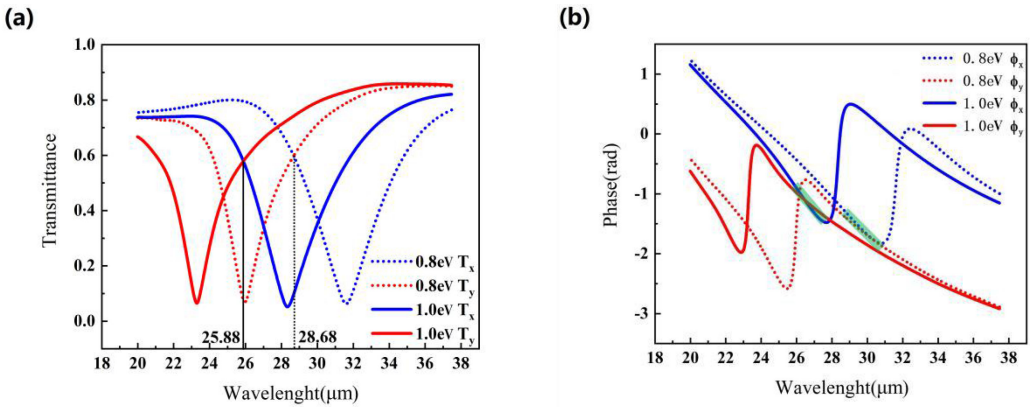

Fig. 7. (a) The transmission coefficient and (b) phase are at different Fermi energies.

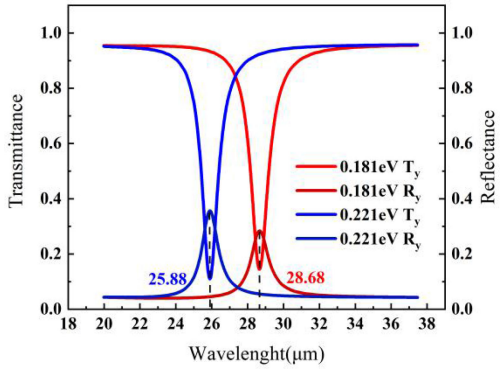

Fig. 8. Filtering efficiency at different Fermi energy.

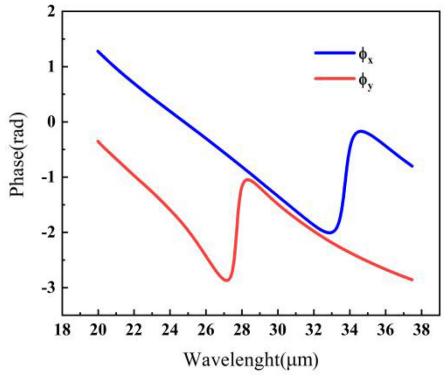

Fig. 9. Phase information at 0.7eV Fermi energy.

Therefore, the polarization resolution structure we designed is a dynamically adjustable structure, which the working wavelength is between 25.88 μm-28.68 μm. We simulate the correspondence between Fermi energy and wavelength in order to match the upper and lower layers. The simulation result is shown in the Fig. 10. Fig. 10(a) shows the correspondence between the quarter-wave plate's central wavelength (where the transmission coefficients of x and y polarized light are the same) and Fermi energy. Fig. 10(b) shows the correspondence between the filter center of the polarization filter and Fermi energy. We can adjust the appropriate Fermi energy so that the upper and lower layers work at the same wavelength.

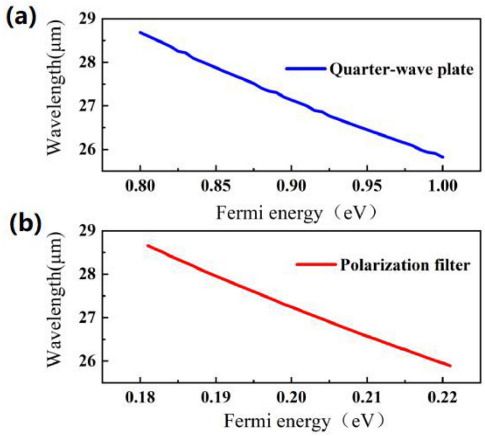

Fig. 10. The correspondence between Fermi energy and wavelength.

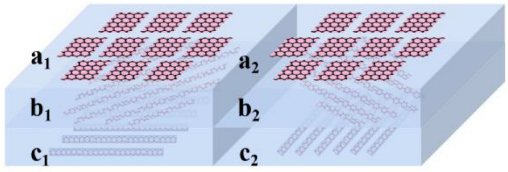

Fig. 11. Full Stokes detection structure.

3.3 Highly Integrated Full Stokes Detection Structure

Next, we propose a full Stokes detection structure. Full Stokes detection can be used for polarization imaging. Stokes vector S is used to represent light with various degrees of polarization, which follow the expression: $S = [S_0, S_1, S_2, S_3]$. The parameter is defined as $S_0 = I$, $S_1 = I_0 - I_{90}$, $S_2 = I_{45} - I_{135}$, $S_3 = I_R - I_L$. Here I is the total intensity, I_0, I_{45}, I_{90}, and I_{135} are the intensity of linearly polarized light with 0°, 45°, 90°, and 135°. IR and IL denote the intensities of the right and left circularly polarized light [19]. Full Stokes detection is to obtain all six light intensity parameters.

Fig. 10 shows the Full Stokes detection structure. The proposed structure has three layers of graphene. Each layer of graphene is individually turned ON and OFF by adjusting the Fermi energy. The combination of a_1 and b_1 is to detect the intensity of RCPL. The combination of a_2 and b_2 is used to detect the intensity of LCPL. c_1, b_1, c_2 and b_2 to detect the intensity of linearly polarized light with 0°, 45°, 90°, and 135°.This makes us obtain the full range of Stokes parameters. Due to the influence of the upper wave plate, the efficiency of the circular polarization detection structure is lower than that of the linear polarization detection structure. Therefore, the detection data needs to be normalized. We denote the normalized data as T', the detection efficiency as T, and the quarter wave plate efficiency as T_p. We need to calculate according to the following formula: $T' = T/T_p$. Thus we can obtain the full Stokes parameters. We integrate all components into two structures. This may conducive to develop high-resolution polarization detectors.

Finally, large-area graphene can grow using chemical vapour deposition on copper an transferred the graphene sheet onto a dielectric substrate. Graphene patterns can be made using lithography. For patch graphene layer, transparent electrodes ion-gel top gates can be adopted to apply bias voltage [20]. For graphene gratings layer, metal electrode can be dopted to apply bias voltage.

4. Conclusion

In conclusion, we have reported the numerical investigation of circular polarization detection in a graphene metasurface by using the finite-difference time-domain (FDTD) method. The function

of the quarter-wave plate and the filter are verified, respectively. By adjusting the Fermi energy levels of the upper and lower graphene layers, the working wavelength can be adjusted freely between 25.88 μm-28.68 μm and similar transmission efficiency can be maintained throughout the operating wavelength range. On this basis, we combined the polarization filter into the structure, which can realize a full Stokes measurement device. Compared with previous studies, the structure has tunability and integration. Our findings are helpful for the development of high-resolution and wide-spectrum polarization detection structures.

Acknowledgements

The authors thank Yuanzhi Zhao, Sitong Shen and Shizhang Ma for helpful discussion. We greatly appreciate the critical support and infrastructure provided for this work by Changchun University of Science and Technology (CUST).

References

[1] M. Khorasaninejad and K B. Crozier, "Silicon nanofin grating as a miniature chirality-distinguishing beam-splitter," *Nature Commun.*, vol. 5, 2014, Art. no. 5386.
[2] D. Lin *et al.*, "Diagnostic potential of polarized surface enhanced Raman pectroscopy technology for colorectal cancer detection," *Opt. Exp.*, vol. 24, no. 3, 2016.
[3] B. L. Meena *et al.*, "Intrinsic fluorescence for cervical precancer detection using polarized light based in-house fabricated portable device," *J. Biomed. Opt.*, vol. 23, no. 1, 2018, Art. no. 015005.
[4] P. Y. Deschamps, J. C. Buriez, F. M. Bréon, G. Sèze, "The POLDER mission: instrument characteristics and scientific objectives," *IEEE Trans. Geosci. Remote Sens.*, vol. 32, no. 3, pp. 598–615, May 1994.
[5] C. Emde, R. Buras1, B. Mayer1, and M. Blumthaler, "The impact of aerosols on polarized sky radiance: Model development, validation, and applications," *Atmospheric Chem. Phys.*, vol. 10, pp. 383–396, 2010
[6] J. Liang et al*et al.*, "Reconfigurable snapshot polarimetric imaging technique through spectral-polarization filtering," *Opt. Lett.*, vol. 44, no. 18, 2019, Art. no. 4574.
[7] F. Liu, Y. Wei, and X. Shao, "Polarization-based exploration for clear underwater vision in natural illumination," *Opt. Exp.*, vol. 27, no. 3, pp. 3629–3641, 2019.
[8] A. Pors, M. G. Nielsen, and S. I. Bozhevolnyi, "Plasmonic metagratings for simultaneous determination of Stokes parameters," *Optica*, vol. 2, no. 8, pp. 716–723, 2015.
[9] F. Ding *et al.*, "Beam-size invariant spectropolarimeters using gap-plasmon metasurfaces," *ACS Photon.*, vol. 2, pp. 943–949, 2017.
[10] S. Wei, Z. Yang, and M. Zhao, "Design of ultracompact polarimeters based on dielectric metasurfaces," *Opt. Lett.*, vol. 42, no. 8, pp. 1580–1583, 2017.
[11] M. Khorasaninejad, W. T. Chen, and F. Capass, "Multispectral chiral imaging with a metalens, nano letters," *Nano Lett.*, vol. 16, pp. 4595−4600, 2016.
[12] P. C. Wu, J. W. Chen, and D. P. Tsai, "Visible metasurfaces for on-chip polarimetry," *ACS Photon.*, vol. 5, pp. 2568−2573, 2018.
[13] A. Basiri, X. Chen, and Y. Yao, "Nature-inspired chiral metasurfaces for circular polarization detection and full-Stokes polarimetric measurements," *Light: Sci. Appl.*, vol. 8, 2019, Art. no. 78.
[14] Z. Liu and B. Bai, "Ultra-thin and high-efficiency graphene metasurface for tunable terahertz wave manipulation," *Opt. Exp.*, vol. 25, no. 8, pp. 8584–8592, 2017.
[15] L. Ju, B. Geng, and F. Wang, "Graphene plasmonics for tunable terahertz metamaterials," *Nature Nanotechnol.*, vol. 6, pp. 630–634, 2011.
[16] Y. Zhang, J. Zhao, and Y. Fu, "Switchable polarization selective terahertz wavefront manipulation in a graphene metasurface," *IEEE Photon. J.*, vol. 11, no. 3, Jun. 2019, Art. no. 4600909.
[17] T. Guo and C. Argyropoulo, "Broadband polarizers based on graphene metasurfaces," *Opt. Lett.*, vol. 41, no. 23, pp. 5592–5595, 2016.
[18] Y. Zhang, L. Ma, and Y. Fu, "Graphene ribbon based tunable terahertz metalens for dual polarization incidences," *Opt. Mater.*, vol. 97, 2019, Art. no. 109325.
[19] E. Arbabi, SM. Kamali, and A. Faraon, "Full Stokes imaging polarimetry using dielectric metasurfaces," *ACS Photon.*, vol. 5, no. 8, Jul. 16, 2018.
[20] L. Ju *et al.*, "Graphene plasmonics for tunable terahertz metamaterials," *Nature Nanotechnol.*, vol. 6, pp. 630–634, Oct. 2011.